

# ACDC: Adaptive Curriculum Planning with Dynamic Contrastive Control for Goal-Conditioned Reinforcement Learning in Robotic Manipulation

Xuerui Wang<sup>1</sup>, Guangyu Ren<sup>2\*</sup>, Tianhong Dai<sup>3</sup>, Bintao Hu<sup>2</sup>, Shuangyao Huang<sup>2</sup>, Wenzhang Zhang<sup>2</sup>, Hengyan Liu<sup>2\*</sup>

<sup>1</sup>Cornell University  
Ithaca, NY 14853, USA

<sup>2</sup>Xi'an Jiaotong-Liverpool University  
Suzhou, China

guangyu.ren@xjtlu.edu.cn, hengyan.liu@xjtlu.edu.cn  
<sup>3</sup>Researcher, Applied Computing

## Abstract

Goal-conditioned reinforcement learning has shown considerable potential in robotic manipulation; however, existing approaches remain limited by their reliance on prioritizing collected experience, resulting in suboptimal performance across diverse tasks. Inspired by human learning behaviors, we propose a more comprehensive learning paradigm, ACDC, which integrates multidimensional Adaptive Curriculum (AC) Planning with Dynamic Contrastive (DC) Control to guide the agent along a well-designed learning trajectory. More specifically, at the planning level, the AC component schedules the learning curriculum by dynamically balancing *diversity*-driven exploration and *quality*-driven exploitation based on the agent's success rate and training progress. At the control level, the DC component implements the curriculum plan through norm-constrained contrastive learning, enabling magnitude-guided experience selection aligned with the current curriculum focus. Extensive experiments on challenging robotic manipulation tasks demonstrate that ACDC consistently outperforms the state-of-the-art baselines in both sample efficiency and final task success rate. Code available: <https://github.com/Xuerui-Wang-oss/Adaptive-Curriculum-Learning-and-Dynamic-Contrastive-Control.git>

## Introduction

Robotic manipulation tasks inherently involve complex planning problems in which agents must reason about achieving desired goals in an environment with sparse feedback (Billard and Kragic 2019). Unlike classical planning that relies on explicit world models (La Valle 2011) or sampling-based planning (Orthey, Chamzas, and Kavraki 2023), goal-conditioned reinforcement learning (GCRL) offers a learning-based planning approach that can achieve multiple goals within the same environment (Liu, Zhu, and Zhang 2022; Schaul et al. 2015). Based on this foundation, Hindsight Experience Replay (HER) (Andrychowicz et al. 2017) significantly advanced GCRL by treating failed trajectories as successful experiences for alternative goals, ef-

fectively densifying the reward signal, and dramatically improving sample efficiency.

Existing research often incorporates prioritization mechanisms such as diversity-based sampling (Dai et al. 2021) or entropy-driven strategies (Zhao and Tresp 2018) to improve experience selection planning in GCRL. However, these approaches typically lack the ability to explicitly guide the agent's learning focus throughout training, particularly in aligning learning signals with the intended curriculum. As a result, agents may waste capacity on suboptimal or irrelevant experiences, especially in sparse environments.

To address these fundamental limitations, we propose a new paradigm, ACDC, a hierarchical planning framework that integrates Adaptive Curriculum Planning with Dynamic Contrastive Control. Rather than directly feeding prioritized experiences to the agent, our approach enables the agent to progress to subsequent curriculum stages only after achieving competency at the current level, while being guided toward curriculum-relevant experiences. As illustrated in Figure 1, our framework comprises two synergistic components: **Adaptive Curriculum (AC) Planning** establishes an adaptive curriculum by evaluating each trajectory's *diversity* and *quality* metrics, dynamically adjusting their weighting based on the agent's success rate and training progress, thus enabling effective curriculum planning without explicit environment modeling; **Dynamic Contrastive (DC) Control** enables the agent to prioritize the experiences most relevant to its current learning objectives derived from its evolving success rate and training progress, while avoiding suboptimal or irrelevant ones. It uses AC's dynamic trajectory scores to construct contrastive pairs and trains an encoder network to distinguish curriculum-relevant experiences (Eysenbach et al. 2022; Zheng et al. 2023). Extensive experiments on challenging robotic manipulation tasks demonstrate that our framework significantly outperforms state-of-the-art experience replay baselines, achieving both superior sample efficiency and final task success rate.

## Related Work

Classical motion planning approaches like RRT (LaValle 1998) and RRT\* (Karaman and Frazzoli 2011) have been widely adopted in robotic manipulation. While these meth-

\*Corresponding authors.

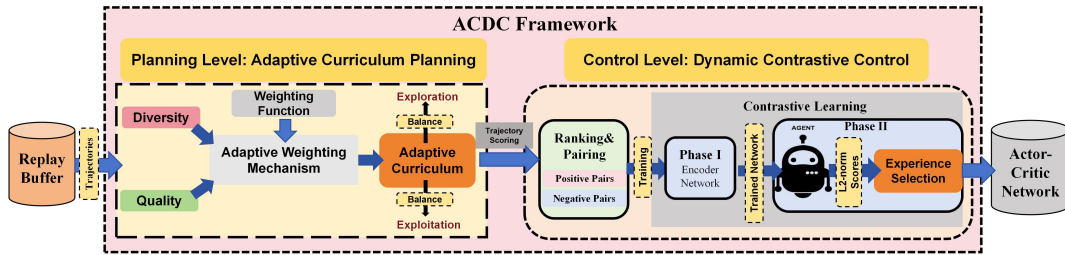


Figure 1: Overview of our ACDC framework. **Planning Level:** Adaptive Curriculum (AC) Planning establishes an adaptive curriculum by combining *diversity* and *quality* metrics through an adaptive weighting mechanism to generate trajectory priority scores  $F(\tau)$ . **Control Level:** Dynamic Contrastive (DC) Control leverages these scores through a ranking and pairing module to construct positive/negative pairs, then employs two-phase contrastive learning for experience selection. Phase I trains an encoder network to learn trajectory representations from constructed pairs, while Phase II computes L2-norm scores through agent-encoder interaction to dynamically guide experience selection.

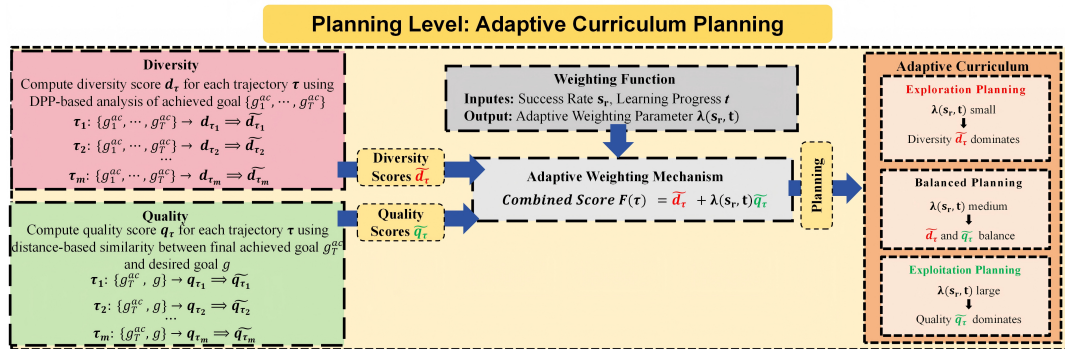


Figure 2: Architecture of Adaptive Curriculum (AC) Planning. The framework evaluates trajectories through two complementary metrics: diversity scores and quality scores, which are normalized to  $\tilde{d}_\tau$  and  $\tilde{q}_\tau$  respectively. The weighting function generates adaptive parameter  $\lambda(s_t, t)$  based on current success rate and learning progress. These components are combined through the adaptive weighting mechanism to produce trajectory scores:  $F(\tau) = \tilde{d}_\tau + \lambda(s_t, t)\tilde{q}_\tau$ , where the value of  $\lambda(s_t, t)$  dynamically determines whether the agent operates in exploration (low  $\lambda(s_t, t)$ ), balanced (medium  $\lambda(s_t, t)$ ), or exploitation (high  $\lambda(s_t, t)$ ) planning. Note: “ $\implies$ ” denotes normalization; achieved goals  $g^{ac}$  refer to task-relevant components extracted from the observation space.

ods provide theoretical guarantees, they require accurate models and struggle with contact-rich tasks (Toussaint 2015; Martín-Martín et al. 2019). Goal-Conditioned Reinforcement Learning (GCRL) offers a fundamentally different approach by reformulating planning as learning a policy that can reach arbitrary goals, eliminating the need for explicit models and replanning (Liu, Zhu, and Zhang 2022).

To further enhance representation learning in GCRL, contrastive learning has emerged as a powerful tool in goal-conditioned settings. Recent work (Eysenbach et al. 2022) demonstrates that contrastive learning can be viewed as a form of goal-conditioned RL, establishing theoretical connections between representation learning and goal-directed robot behavior. Methods like CURL (Laskin, Srinivas, and Abbeel 2020) and RIG (Nair et al. 2018) have also shown that contrastive approaches can significantly improve sample efficiency through better representation learning in visual goal-conditioned tasks.

In recent years, researchers have begun to recognize the synergistic potential between curriculum learning and

HER (Andrychowicz et al. 2017) in GCRL, leading to several notable integration attempts. CHER (Curriculum-guided Hindsight Experience Replay) (Fang et al. 2019) represents a pioneering effort in this direction, dynamically adjusting the proportion of curiosity-driven exploration in the reward function during training. By balancing between achieving original goals and exploring diverse outcomes, CHER demonstrates improved sample efficiency compared to standard HER.

Beyond explicit curriculum learning, other methods have been developed to enhance experience selection in HER to improve the sample efficiency of GCRL. DTGSH (Dai et al. 2021) focuses on selecting various hindsight goals through determinantal point processes (Borodin 2009), ensuring that replayed experiences cover a wide range of goal configurations. Similarly, FAHER (Kim et al. 2024) uses clustering to enhance sampling efficiency by focusing on potential-insight episodes.

While these various approaches have shown promise in improving GCRL through different selection strategies,

none have systematically integrated curriculum scheduling with contrastive learning for experience selection. Our work addresses this gap by coordinating adaptive curriculum planning with contrastive control: the framework automatically identifies and prioritizes trajectories most beneficial to the agent’s current success rate and learning progress through curriculum-guided contrastive learning.

## Preliminaries

### Goal-Conditioned Reinforcement Learning

Goal-conditioned reinforcement learning (GCRL) extends the standard Markov Decision Process (MDP) (Puterman 1994) to a goal-conditioned MDP  $(S, A, P, R, G, \gamma)$ , where  $S$  is the state space,  $A$  is the action space,  $P$  is the state transition probability,  $R$  is the reward function,  $G$  is the goal space, and  $\gamma$  is the discount factor.

We define a mapping function  $\phi : S \rightarrow G$  that maps a state  $s \in S$  to a corresponding achieved goal  $g^{ac} = \phi(s) \in G$ . In GCRL, goals  $g \in G$  represent desired configurations in the task space, and the agent learns a policy  $\pi(a|s, g)$  (Schaul et al. 2015) that maps state-goal pairs to actions. The core principle is to condition both policy and value functions on goals, enabling multi-task learning within the same environment. The reward function typically takes a sparse binary form:

$$r(s_t, a_t, g) = R(\phi(s_{t+1}), g) = \begin{cases} 0 & \text{if } \|\phi(s_{t+1}) - g\| \leq \epsilon, \\ -1 & \text{otherwise,} \end{cases} \quad (1)$$

where  $\phi(s_{t+1})$  (or  $g_{t+1}^{ac}$ ) represents the achieved goal after taking action  $a_t$  in state  $s_t$ , and  $\epsilon$  is a tolerance threshold. This goal-conditioning mechanism transforms the learning process from single-task optimization to multi-goal generalization.

### Hindsight Experience Replay

While GCRL provides a framework for multi-goal learning, the fundamental sparse reward challenge persists when the agent fails to reach the desired goals (Liu, Zhu, and Zhang 2022). HER (Andrychowicz et al. 2017) further addresses this limitation through goal relabeling, which retrospectively treats failed trajectories as successful experiences for alternative goals.

Given a trajectory  $\tau = (s_0, a_0, s_1, a_1, \dots, s_T)$  with desired goal  $g$ , HER performs goal relabeling by substituting  $g$  with achieved goals from the trajectory (Andrychowicz et al. 2017). The achieved goal  $g_t^{ac}$  is extracted from the state  $s_t$  via the mapping  $\phi$ . Specifically, for each transition  $(s_t, a_t, s_{t+1}, r_t, g)$ , HER generates additional experiences:

$$(s_t, a_t, s_{t+1}, R(g_{t+1}^{ac}, g'), g'), \quad (2)$$

where  $g'$  is selected from future achieved goals  $\{g_{t+k}^{ac} | k \geq 1\}$  in the trajectory, and  $g_{t+1}^{ac}$  represents the achieved goal at time step  $t + 1$ .

### Contrastive Representation Learning

Contrastive representation learning (Eysenbach et al. 2022) uses positive and negative examples to learn meaningful representations. The goal is to learn representations such that

positive pairs have similar representations while negative pairs have dissimilar representations. The core InfoNCE loss function (van den Oord, Li, and Vinyals 2018) is:

$$\mathcal{L}_{\text{contrastive}} = -\log \frac{\exp(\text{sim}(f_\theta(x), f_\theta(x^+))/\alpha)}{\sum_i \exp(\text{sim}(f_\theta(x), f_\theta(x_i))/\alpha)}, \quad (3)$$

where  $f_\theta(\cdot)$  is an encoder,  $x$  is an anchor sample,  $x^+$  represents positive examples,  $x_i$  includes both positive and negative examples,  $\text{sim}(\cdot, \cdot)$  measures similarity, and  $\alpha$  is a temperature parameter.

## Methodology

### Adaptive Curriculum Planning (AC)

As illustrated in Figure 2, the AC module progressively schedules learning tasks by dynamically balancing the transition from exploration to exploitation, thereby constructing a performance-aware curriculum that enhances policy learning efficiency. It achieves this by jointly evaluating each trajectory’s *diversity*, to encourage broad exploration, and *quality*, to promote goal achievement. These criteria are dynamically adjusted through a task-adaptive weighting function based on the agent’s success rates and training progress. As a result, curriculum planning evolves in tandem with the agent’s capabilities, ensuring that experience replay remains focused, balanced, and efficient throughout the learning process.

### Trajectory Evaluation Metrics

**Diversity score** quantifies how varied a trajectory is in terms of the state space or goal space it explores. Diverse trajectories expose the agent to a broader range of environmental states and behaviors, providing richer information and promoting better generalization. Inspired by the work (Dai et al. 2021), we employ *determinantal point processes (DPPs)* (Borodin 2009; Kulesza and Taskar 2012) to measure trajectory diversity in a principled manner. We first divide a trajectory  $\tau$  into overlapping partial trajectories using a sliding window of size 2:

$$\mathcal{T} = \left\{ \underbrace{\{g_1^{ac}, g_2^{ac}\}}_{\tau_1}, \underbrace{\{g_2^{ac}, g_3^{ac}\}}_{\tau_2}, \dots, \underbrace{\{g_{T-1}^{ac}, g_T^{ac}\}}_{\tau_{T-1}} \right\}. \quad (4)$$

For each partial trajectory  $\tau_j$ , we compute its diversity using the determinant of the kernel matrix (Kulesza and Taskar 2012):

$$d_{\tau_j} = \det(L_{\tau_j}), \text{ where } L_{\tau_j} = \hat{G}_j^T \hat{G}_j, \quad (5)$$

$\hat{G}_j = [\hat{g}_j^{ac}, \hat{g}_{j+1}^{ac}]$  contains the normalized achieved goals. The overall trajectory diversity is:

$$d_\tau = \sum_{j=1}^{T-1} d_{\tau_j}. \quad (6)$$

Then we normalize the score via min-max scaling:  $\tilde{d}_\tau = \frac{d_\tau - d_{\min}^{\mathcal{B}}}{d_{\max}^{\mathcal{B}} - d_{\min}^{\mathcal{B}}}$ , where  $d_{\min}^{\mathcal{B}} = \min_{\tau' \in \mathcal{B}} d_{\tau'}$  and  $d_{\max}^{\mathcal{B}} = \max_{\tau' \in \mathcal{B}} d_{\tau'}$  are the minimum and maximum diversity scores in the current replay buffer  $\mathcal{B}$ .

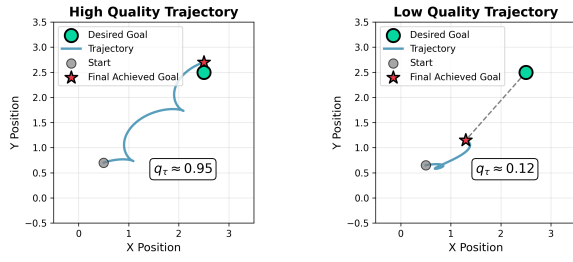


Figure 3: Quality score measures how close a trajectory’s final achieved goal is to the desired goal. The score uses a Gaussian function to transform Euclidean distance into a value between 0 and 1, providing smooth differentiation between successful and unsuccessful trajectories.

**Quality Score** quantifies how close a trajectory comes to achieving its desired goal by using a *distance-based similarity measure* (Liu, Zhu, and Zhang 2022):

$$\tilde{q}_\tau = \exp\left(-\frac{(\|g_T^{ac} - g\|_2)^2}{2\sigma^2}\right), \quad (7)$$

where  $g_T^{ac}$  is the final achieved goal,  $g$  is the desired goal,  $\|\cdot\|_2$  denotes the L2 norm, and  $\sigma = 0.2$  controls sensitivity. Figure 3 illustrates this concept. The quality score ranges from 0 to 1, where values closer to 1 indicate that the trajectory’s final achieved goal is near the desired goal (high-quality trajectory, left panel:  $\tilde{q}_\tau \approx 0.95$ ), while values closer to 0 indicate the final achieved goal is far from the target (low-quality trajectory, right panel:  $\tilde{q}_\tau \approx 0.12$ ).

**Adaptive Weighting Mechanism** The key innovation in AC is the adaptive weighting (Lin et al. 2019) between *diversity* and *quality* scores. We combine these metrics using:

$$F(\tau) = \tilde{d}_\tau + \lambda(s_r, t) \cdot \tilde{q}_\tau, \quad (8)$$

where  $\lambda(s_r, t)$  is our adaptive weighting function that responds to both the agent’s success rate  $s_r$  and training progress  $t$ .

Unlike fixed curriculum schedules (Bengio et al. 2009; Florensa et al. 2017), our adaptive function adjusts  $\lambda(s_r, t)$  based on the agent’s actual performance in the specific task:

$$\lambda(s_r, t) = \lambda_0 \cdot (1 + \eta(s_r))^t, \quad (9)$$

where  $\lambda_0$  is the initial weight and  $\eta(s_r)$  is an adaptive growth rate that controls how quickly the weighting shifts from diversity to quality:

$$\eta(s_r) = \begin{cases} \eta_{base} \cdot 0.5, & \text{if } s_r < \theta_{low} \\ \eta_{base}, & \text{if } \theta_{low} \leq s_r \leq \theta_{high} \\ \eta_{base} \cdot 2.0, & \text{if } s_r > \theta_{high}, \end{cases} \quad (10)$$

where  $\eta_{base} = 0.01$ , and the thresholds are selected based on simulation results shown in Figure 12. The adaptive parameter  $\eta(s_r)$  implements a three-tier strategy that controls the exponential growth rate:

- **Struggling phase** ( $s_r < \theta_{low}$ ): Slow growth allows the agent to maintain diversity-focused sampling longer for extended exploration.

---

### Algorithm 1: Adaptive Curriculum Planning

---

- 1: **Input:** Replay buffer  $\mathcal{B}$ , current success rate  $s_r$ , training step  $t$
  - 2: **Parameter:**  $\alpha = 0.7$  (EMA smoothing factor),  $\lambda_0 = 0.1$  (initial weight)
  - 3: **Initialize:**  $\eta_{previous} = \eta_{base}$  (at  $t = 0$ )
  - 4: **Output:** Combined scores  $\{F(\tau_i)\}_{i=1}^{|\mathcal{B}|}$
  - 5: Compute target learning rate  $\eta_{target}$  based on  $s_r$  using Eq. (10)
  - 6:  $\eta_{current} \leftarrow \alpha \cdot \eta_{target} + (1 - \alpha) \cdot \eta_{previous}$  // **EMA update**
  - 7: Compute adaptive weight:  $\lambda(s_r, t) \leftarrow \lambda_0 \cdot (1 + \eta_{current})^t$
  - 8: **for** each trajectory  $\tau_i \in \mathcal{B}$  **do**
  - 9:    $\tilde{d}_{\tau_i} \leftarrow$  Compute diversity( $\tau_i$ ) score using Eq. (6)
  - 10:    $\tilde{q}_{\tau_i} \leftarrow$  Compute quality( $\tau_i$ ) score using Eq. (7)
  - 11:    $F(\tau_i) \leftarrow \tilde{d}_{\tau_i} + \lambda(s_r, t) \cdot \tilde{q}_{\tau_i}$  // **Combined score**
  - 12: **end for**
  - 13: Update:  $\eta_{previous} \leftarrow \eta_{current}$  for next iteration
  - 14: **return**  $\{F(\tau_i)\}_{i=1}^{|\mathcal{B}|}$
- 

- **Learning phase** ( $\theta_{low} \leq s_r \leq \theta_{high}$ ): Standard growth provides the agent with balanced exploration-exploitation.
- **Mastery phase** ( $s_r > \theta_{high}$ ): Accelerated growth enables the agent to rapidly shift toward quality-focused sampling.

However, abrupt transitions between phases can cause training instability when success rates fluctuate around thresholds  $\theta_{low}$  and  $\theta_{high}$ . To address this instability (Matisen et al. 2019), we employ EMA (Haynes, Corns, and Venayagamoorthy 2012) in Algorithm 1 to prevent oscillations and ensure stable transitions between modes.

Crucially, the hyperparameters governing the components—including the sliding window size in Eq (4), sensitivity  $\sigma$  in Eq (7), and the growth factors in Eq (11)—were determined empirically via grid search. We provide the full sensitivity analysis and search ranges in the **Appendix A** to demonstrate their robustness.

### Dynamic Contrastive Control (DC)

As illustrated in Figure 4, the DC mechanism executes AC’s curriculum plan (Algorithm 1) at the operational level through learned trajectory representations. Specifically, DC trains a contrastive encoder guided by AC’s trajectory scores  $F(\tau)$ , enabling the agent to identify and prioritize experiences most relevant to its current learning stage  $(s_r, t)$ , while steering away from suboptimal or irrelevant ones.

**Dynamic Contrastive Pairing** We leverage the combined scores  $F(\tau)$  from the AC module to form contrastive trajectory pairs (Eysenbach et al. 2022). Unlike conventional methods that use fixed augmentations (Chen et al. 2020), our method dynamically segregates trajectories according to their current priority scores.

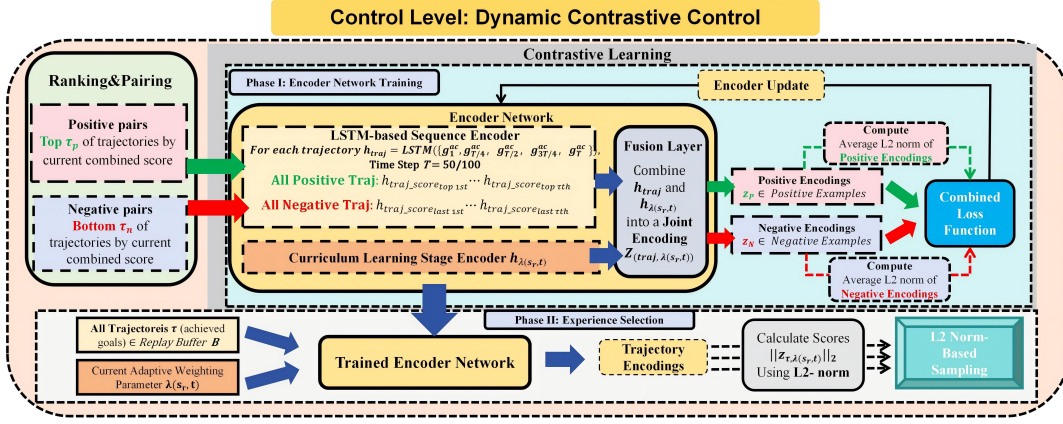


Figure 4: Architecture of Dynamic Contrastive (DC) Control. This level operates in two phases: **Phase I (Encoder Network Training)** ranks trajectories using AC’s combined scores  $F(\tau)$  and selects positive and negative pairs. An LSTM-based sequence encoder extracts temporal features from achieved goals along the trajectory and fuses them with the adaptive weighting parameter  $\lambda(s_r, t)$  through a fusion layer to create joint encodings  $Z_{(\tau, \lambda(s_r, t))}$ , then employs contrastive learning with a combined loss function to separate positive and negative examples while ensuring positive encodings exhibit larger norms than negative ones. **Phase II (Experience Selection)** uses the trained encoder network to process all trajectories  $\tau \in$  current Replay Buffer  $\mathcal{B}$  with  $\lambda(s_r, t)$ , computing L2-norms  $\|Z_{\tau, \lambda(s_r, t)}\|_2$  as trajectory scores for dynamic experience selection that adapts to the agent’s evolving capabilities.

$$\mathcal{P}_{\lambda(s_r, t)} = \{\tau \in \mathcal{B} \mid F(\tau) \in \text{top-}\tau_p \text{ of all current } F(\tau)\}, \quad (11)$$

$$\mathcal{N}_{\lambda(s_r, t)} = \{\tau \in \mathcal{B} \mid F(\tau) \in \text{bottom-}\tau_n \text{ of all current } F(\tau)\}, \quad (12)$$

where  $\tau_p$  and  $\tau_n$  denote the sample size thresholds for positive and negative sets respectively ( $\tau_p/\tau_n = 0.3$  in our experiments). The pairing process dynamically adapts as  $\lambda(s_r, t)$  evolves during training, continuously redefining positive and negative sample selection based on the agent’s current learning stage.

### Phase I: Encoder Network Training

**Encoder Network** Our encoder adopts a fusion design that integrates trajectory dynamics with curriculum context. To balance representational richness and computational efficiency, we extract key frames based on achieved goals at strategic points along the trajectory:

$$\mathcal{K} = \{g_{t_0}^{ac}, g_{t_1}^{ac}, g_{t_2}^{ac}, g_{t_3}^{ac}, g_{t_4}^{ac}\}, \quad (13)$$

where  $g_{t_i}^{ac}$  denotes the achieved goal at time  $t_i$ , with  $t_0 = 0$  (start),  $t_1 = T/4$  (early phase),  $t_2 = T/2$  (middle phase),  $t_3 = 3T/4$  (late phase), and  $t_4 = T$  (final achieved goal).

The network produces joint encodings that fuse trajectory features with current curriculum information:

$$z_{\tau, \lambda(s_r, t)} = f_{\text{encoder}}(\tau, \lambda(s_r, t)) = W_f[h_{\text{traj}}; h_{\lambda(s_r, t)}] + b_f, \quad (14)$$

where  $h_{\text{traj}} = \text{LSTM}(\mathcal{K})$  (Han et al. 2024) and  $h_{\lambda(s_r, t)} = W_\lambda \lambda(s_r, t) + b_\lambda$  embeds the current curriculum stage  $(s_r, t)$ . This fusion ensures that identical trajectories yield different

representations at different learning stages, capturing their changing value as the agent progresses.

We employ an LSTM as the feature extractor specifically to capture the temporal evolution of trajectories within this fusion architecture. Empirically, the LSTM proved highly stable and effective for this objective, outperforming alternatives like GRUs (Dey and Salem 2017) or 1D-CNNs (Yamashita et al. 2018) in our preliminary evaluations.

**Norm-Constrained Contrastive Learning** The contrastive framework constructs a structured representation space that serves two purposes: it separates high- and low-value trajectories into distinct regions and encodes trajectory importance via representation magnitude.

A modified InfoNCE loss (van den Oord, Li, and Vinyals 2018) is implemented with an explicit norm constraint:

$$\mathcal{L}_{\text{total}} = \mathcal{L}_{\text{con}}(z_{\mathcal{P}, \lambda(s_r, t)}, z_{\mathcal{N}, \lambda(s_r, t)}) + \alpha \mathcal{L}_{\text{norm}}(\mu_{\mathcal{P}}, \mu_{\mathcal{N}}), \quad (15)$$

where  $z_{\mathcal{P}, \lambda(s_r, t)} = \{z_{\tau, \lambda(s_r, t)} : \tau \in \mathcal{P}_{\lambda(s_r, t)}\}$  and  $z_{\mathcal{N}, \lambda(s_r, t)} = \{z_{\tau, \lambda(s_r, t)} : \tau \in \mathcal{N}_{\lambda(s_r, t)}\}$  denote the sets of positive and negative joint encodings respectively. The terms  $\mu_{\mathcal{P}} = \frac{1}{|\mathcal{P}_{\lambda(s_r, t)}|} \sum_{\tau \in \mathcal{P}_{\lambda(s_r, t)}} \|z_{\tau, \lambda(s_r, t)}\|_2$  and  $\mu_{\mathcal{N}} = \frac{1}{|\mathcal{N}_{\lambda(s_r, t)}|} \sum_{\tau \in \mathcal{N}_{\lambda(s_r, t)}} \|z_{\tau, \lambda(s_r, t)}\|_2$  represent the average L2 norms of the positive and negative encoding sets respectively. The weighting factor  $\alpha$  balances the contrastive alignment and norm-based ranking objectives.

**Self-anchored Contrastive Component:** The contrastive loss function first L2-normalizes all input encodings, then employs a self-anchored variant of InfoNCE (van den Oord, Li, and Vinyals 2018):

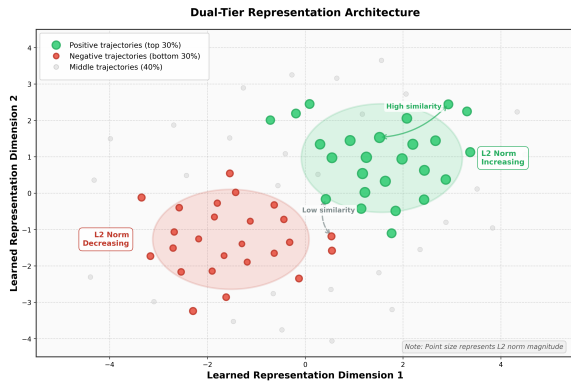


Figure 5: The trained encoder network establishes a two-tier representation architecture. Positive trajectories occupy the premium region (green) while negative trajectories are confined to the inferior region (red), with point size indicating L2 norm magnitude. This structure enables both categorical separation and magnitude-based importance ranking.

$$\mathcal{L}_{\text{con}} = -\frac{1}{|\mathcal{P}_{\lambda(s_r, t)}|} \sum_{i=1}^{|\mathcal{P}_{\lambda(s_r, t)}|} \log \frac{e^{(\bar{z}_i \cdot \bar{z}_i / \alpha)}}{\sum_{j=1}^{|\mathcal{P}_{\lambda(s_r, t)}| + |\mathcal{N}_{\lambda(s_r, t)}|} e^{(\bar{z}_i \cdot \bar{z}_j / \alpha)}}, \quad (16)$$

where  $\bar{z}_i$  and  $\bar{z}_j$  denote the L2-normalized encodings of the  $i$ -th positive trajectory and all sample trajectories, respectively.

The self-similarity term  $\bar{z}_i \cdot \bar{z}_i$  acts as a fixed confidence baseline, ensuring each positive trajectory functions as an *independent anchor*. This explicitly prevents feature collapse among successful trials, thereby preserving the topological diversity essential for the AC module.

**Norm Constraint Component:** To enhance informative trajectories in the premium region and suppress those in the inferior region, a magnitude-based adjustment mechanism is introduced:

$$\mathcal{L}_{\text{norm}} = \max(0, \mu_{\mathcal{N}} - \mu_{\mathcal{P}} + m). \quad (17)$$

This constraint ensures that positive trajectories maintain consistently higher signal strength than negative trajectories by at least the margin  $m$  (Hadsell, Chopra, and LeCun 2006), systematically pushing premium-region trajectories to exhibit larger magnitudes than inferior-region trajectories.

Following the optimization procedure, the trained encoder network produces a structured representation space with clear dual-tier architecture, as illustrated in Figure 5.

## Phase II: Experience Selection

**Magnitude-Guided Sampling** Using the trained encoder of Phase I, all trajectories in the replay buffer are processed to compute magnitude-guided sampling probabilities (Wu et al. 2024).

For each trajectory  $\tau \in \mathcal{B}$ , a joint encoding  $z_{\tau, \lambda(s_r, t)}$  is computed based on the current curriculum stage  $\lambda(s_r, t)$ .

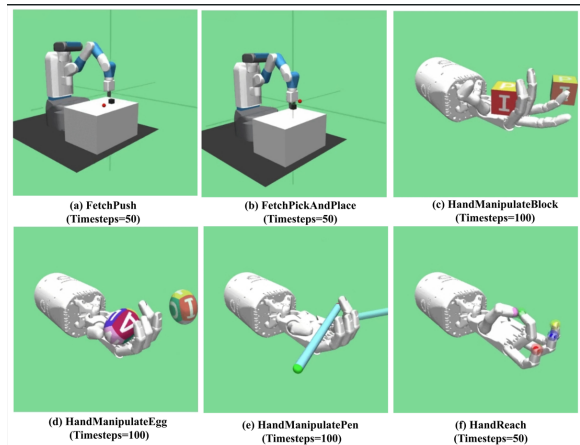


Figure 6: Fetch and Shadow Dexterous Hand environments.

The L2 norm of this encoding is used as an importance measure (Schaul et al. 2016).

$$P_{\text{contrastive}}(\tau) = \frac{\|z_{\tau, \lambda(s_r, t)}\|_2}{\sum_{\tau' \in \mathcal{B}} \|z_{\tau', \lambda(s_r, t)}\|_2}. \quad (18)$$

This magnitude-guided sampling operationalizes AC’s curriculum plan, seamlessly translating high-level diversity-quality objectives into concrete experience selection through learned trajectory representations.

## Experiments

ACDC is evaluated on six robotic manipulation tasks from the OpenAI Gym benchmark (Brockman et al. 2016), as shown in Figure 6. These tasks span two robotic platforms with varying complexity: **Fetch environments** using a 7-DoF robotic arm (4-dimensional action space) and **Shadow Dexterous Hand environments** with 24 degrees of freedom (20-dimensional action space).

### Training Settings

Our training setup follows the standard HER framework (Andrychowicz et al. 2017) with MPI parallelization using 10 workers for parallel experience collection. The agent is trained for 100 epochs. In each epoch, we collect 50 cycles of experience, where each cycle gathers 20 episodes in parallel (2 rollouts per worker  $\times$  10 workers), resulting in 1,000 episodes per epoch and 100,000 episodes in total.

For ACDC-specific components, the contrastive encoder uses a learning rate of  $\eta_{\text{base}} = 0.001$  and is updated every 5 policy gradient steps. The environment-specific thresholds for the adaptive weighting mechanism are configured as follows:

- Fetch manipulation:  $\theta_{\text{low}} = 0.3, \theta_{\text{high}} = 0.65$ .
- Hand manipulation (Full Goal-Type):  $\theta_{\text{low}} = 0.3, \theta_{\text{high}} = 0.65$ .
- Hand manipulation (Rotate Goal-Type):  $\theta_{\text{low}} = 0.25, \theta_{\text{high}} = 0.35$ .

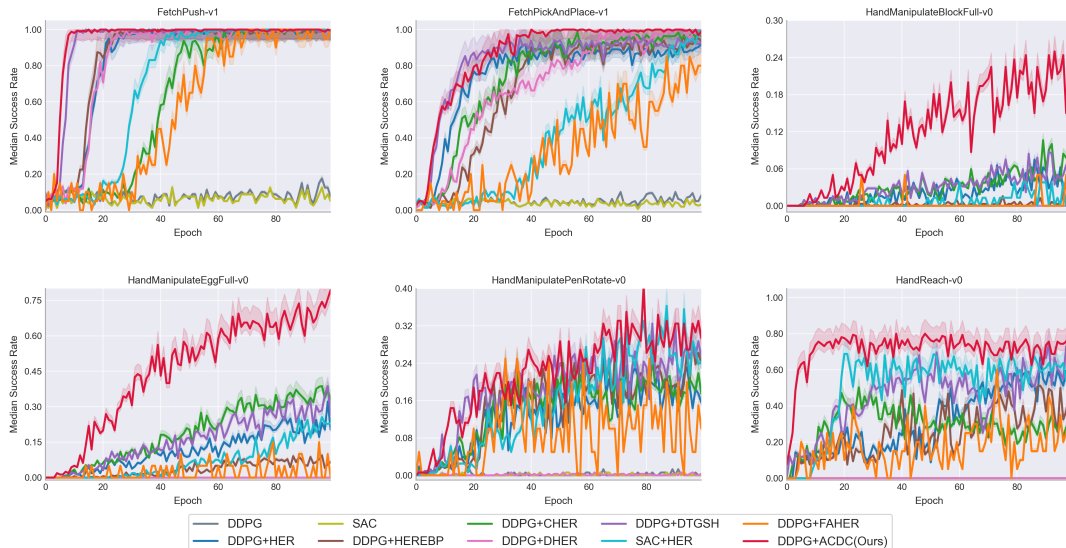


Figure 7: Learning curves showing median success rate across 5 random seeds in six robotic manipulation environments.

Table 1: Final mean success rate  $\pm$  standard deviation averaged over the last 20 epochs. Best results are shown in **bold**.

| Method                              | Venue        | Push                            | Pick&Place                      | BlockFull                       | EggFull                         | PenRotate                       | HandReach                       |
|-------------------------------------|--------------|---------------------------------|---------------------------------|---------------------------------|---------------------------------|---------------------------------|---------------------------------|
| DDPG (Lillicrap et al. 2015)        | -            | 0.09 $\pm$ 0.04                 | 0.07 $\pm$ 0.02                 | 0.00 $\pm$ 0.00                 | 0.00 $\pm$ 0.00                 | 0.00 $\pm$ 0.00                 | 0.00 $\pm$ 0.00                 |
| DDPG+HER (Andrychowicz et al. 2017) | NeurIPS'17   | 0.99 $\pm$ 0.01                 | 0.88 $\pm$ 0.02                 | 0.04 $\pm$ 0.02                 | 0.22 $\pm$ 0.04                 | 0.18 $\pm$ 0.03                 | 0.54 $\pm$ 0.05                 |
| DDPG+HEREBP (Zhao and Tresp 2018)   | CoRL'18      | 0.99 $\pm$ 0.01                 | 0.94 $\pm$ 0.02                 | 0.00 $\pm$ 0.00                 | 0.07 $\pm$ 0.02                 | 0.24 $\pm$ 0.03                 | 0.42 $\pm$ 0.05                 |
| SAC (Haarnoja et al. 2018)          | ICML'18      | 0.07 $\pm$ 0.03                 | 0.03 $\pm$ 0.01                 | 0.00 $\pm$ 0.00                 | 0.00 $\pm$ 0.00                 | 0.00 $\pm$ 0.00                 | 0.00 $\pm$ 0.00                 |
| DDPG+DHER (Fang et al. 2018)        | ICLR'18      | 0.99 $\pm$ 0.01                 | 0.97 $\pm$ 0.03                 | 0.00 $\pm$ 0.00                 | 0.00 $\pm$ 0.00                 | 0.00 $\pm$ 0.00                 | 0.00 $\pm$ 0.00                 |
| DDPG+CHER (Fang et al. 2019)        | NeurIPS'19   | 0.99 $\pm$ 0.01                 | 0.97 $\pm$ 0.01                 | 0.07 $\pm$ 0.02                 | 0.33 $\pm$ 0.02                 | 0.18 $\pm$ 0.02                 | 0.28 $\pm$ 0.03                 |
| DDPG+DTGSH (Dai et al. 2021)        | PRICAI'21    | <b>1.00<math>\pm</math>0.00</b> | 0.93 $\pm$ 0.02                 | 0.07 $\pm$ 0.02                 | 0.29 $\pm$ 0.05                 | 0.25 $\pm$ 0.04                 | 0.62 $\pm$ 0.04                 |
| SAC+HER(Lee and Moon 2023)          | ICT Expr.'23 | <b>1.00<math>\pm</math>0.00</b> | 0.87 $\pm$ 0.10                 | 0.02 $\pm$ 0.02                 | 0.20 $\pm$ 0.04                 | 0.27 $\pm$ 0.04                 | 0.60 $\pm$ 0.05                 |
| DDPG+FAHER (Kim et al. 2024)        | PeerJ CS'24  | 0.98 $\pm$ 0.03                 | 0.78 $\pm$ 0.04                 | 0.00 $\pm$ 0.00                 | 0.04 $\pm$ 0.03                 | 0.12 $\pm$ 0.05                 | 0.22 $\pm$ 0.09                 |
| DDPG+ACDC (Ours)                    | -            | <b>1.00<math>\pm</math>0.00</b> | <b>1.00<math>\pm</math>0.00</b> | <b>0.25<math>\pm</math>0.04</b> | <b>0.69<math>\pm</math>0.05</b> | <b>0.28<math>\pm</math>0.04</b> | <b>0.72<math>\pm</math>0.04</b> |

## Benchmark Results

We evaluate ACDC against several online GCRL baselines in sparse reward environments, including DDPG-based and SAC-based methods: DDPG (Lillicrap et al. 2015), DDPG+HER (Andrychowicz et al. 2017), SAC (Haarnoja et al. 2018), DDPG+HEREBP (Zhao and Tresp 2018), DDPG+DHER (Fang et al. 2018), DDPG+CHER (Fang et al. 2019), DDPG+DTGSH (Dai et al. 2021), SAC+HER (Lee and Moon 2023), and DDPG+FAHER (Kim et al. 2024).

Figure 7 and Table 1 demonstrate ACDC’s superior performance across all environments. In Fetch tasks, ACDC achieves perfect performance, with particularly notable success in PickAndPlace where it is the only method to reach **1.00 $\pm$ 0.00**. The most remarkable improvements occur in challenging Hand manipulation tasks characterized by high-dimensional goal spaces, where ACDC achieves significant gains in EggFull and BlockFull, substantial improvements in HandReach. Moreover, for the BlockFull task, extended training (250 epochs) confirms that ACDC achieves stable convergence with a success rate of **0.38 $\pm$ 0.04**, in sharp contrast to baselines that fail to overcome the exploration bottleneck (see [Appendix B.1](#)).

To further validate these findings, we provide a comprehensive quantitative analysis of Sample Efficiency using *Time-to-Threshold (TTT)* and *Cumulative Regret* (Sutton, Barto et al. 1998) in Table 2, with a detailed analysis provided in [Appendix B.2](#). Additionally, we integrate ACDC with the SAC agent to demonstrate the framework’s algorithmic universality in [Appendix B.3](#).

## Ablation Studies

**Component Contribution Analysis** We analyze the contribution of each component: DDPG+AC-D (diversity-only curriculum planning), DDPG+AC-Q (quality-only curriculum planning), DDPG+AC (adaptive curriculum only), and DDPG+ACDC in Hand environments. As shown in Figure 8, DDPG+ACDC consistently outperforms all variants throughout training.

This reveals that AC and DC are indispensable for agent’s efficiency learning. AC, acting as the ‘Planner’, provides essential trajectory guidance by scoring experiences based on the agent’s current learning stage ( $s_t, t$ ). Without AC, the agent would lack a principled criterion to distinguish which experiences are valuable for the current curriculum stage. Simultaneously, DC, acting as the ‘Executor’, utilizes these

Table 2: Sample Efficiency Analysis across 6 Robotic Tasks. For each environment, we set a specific success rate threshold  $\theta$  (in 2nd column) and report the Time-to-Threshold (TTT), defined as the number of epochs required to first reach  $\theta$ . We also report the Cumulative Regret ( $R$ ) over 100 epochs based on the learning curves. Lower values for both metrics indicate higher sample efficiency. “-” denotes failure to reach  $\theta$  within the training budget.

| Environment                       | Threshold ( $\theta$ ) | Time-to-Threshold (Epochs) $\downarrow$ |        |       |      |           | Cumulative Regret ( $R$ ) $\downarrow$ |        |       |      |             |
|-----------------------------------|------------------------|---|--------|-------|------|-----------|--|--------|-------|------|-------------|
|                                   |                        | HER                                     | HEREBP | DTGSH | CHER | ACDC      | HER                                    | HEREBP | DTGSH | CHER | ACDC        |
| <i>FetchPush-v1</i>               | 0.95                   | 25                                      | 18     | 14    | 60   | <b>8</b>  | 22.4                                   | 19.8   | 16.5  | 28.7 | <b>8.5</b>  |
| <i>FetchPickAndPlace-v1</i>       | 0.90                   | 35                                      | 85     | 40    | 42   | <b>18</b> | 38.5                                   | 48.5   | 41.2  | 45.3 | <b>18.2</b> |
| <i>HandReach-v0</i>               | 0.50                   | 65                                      | -      | 35    | -    | <b>5</b>  | 68.2                                   | 75.2   | 60.5  | 82.1 | <b>44.1</b> |
| <i>HandManipulateEggFull-v0</i>   | 0.30                   | -                                       | -      | 78    | 63   | <b>23</b> | 88.2                                   | 92.1   | 81.7  | 80.5 | <b>62.8</b> |
| <i>HandManipulatePenRotate-v0</i> | 0.20                   | 32                                      | 43     | 22    | 40   | <b>15</b> | 89.4                                   | 91.3   | 86.2  | 88.9 | <b>81.5</b> |
| <i>HandManipulateBlockFull-v0</i> | 0.20                   | -                                       | -      | -     | -    | <b>75</b> | 97.2                                   | 98.1   | 96.5  | 95.1 | <b>88.5</b> |

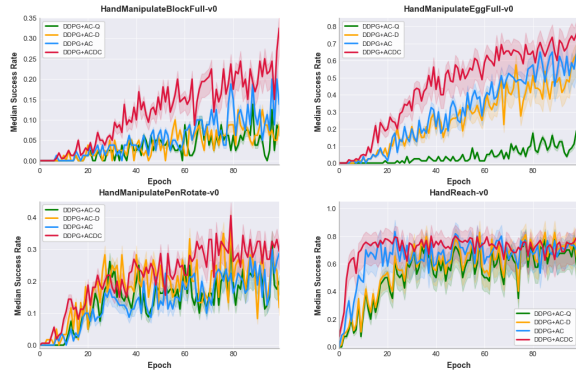


Figure 8: Performance evaluation of individual components versus the complete ACDC framework.

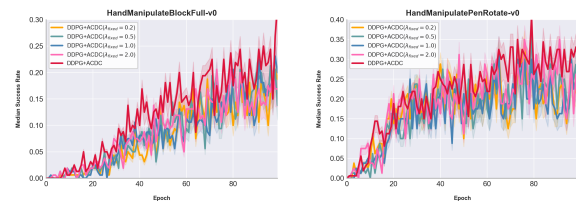


Figure 9: Performance comparison between fixed  $\lambda_{fixed}$  and adaptive  $\lambda(s_r, t)$  weighting mechanism.

scores to strictly partition positive and negative samples, thereby constructing a structured representation space.

AC establishes curriculum priorities, however, its explicit scores lack the representational capacity to effectively filter experiences at an operational level. DC addresses this by translating high-level planning into precise experience selection through learned representations, ensuring that the agent’s learning focus remains strictly aligned with the intended curriculum.

**Adaptive Weighting Mechanism Analysis** We evaluate the effectiveness of our weighting function by comparing fixed parameter configurations ( $\lambda_{fixed} = 0.2, 0.5, 1.0, 2.0$ ) against our adaptive  $\lambda(s_r, t)$ .

Unlike fixed parameters, which force a static trade-off, our adaptive  $\lambda(s_r, t)$  acts as a dynamic regulator. As shown in Figure 9, fixed weights (e.g.,  $\lambda_{fixed} = 0.2$  or  $\lambda_{fixed} = 2.0$ ) lack the flexibility to adapt across varying task complexities.

In contrast, our adaptive weighting function delivers performance that is competitive with, and often superior to, the most effective fixed parameter settings. This demonstrates that our mechanism  $\lambda(s_r, t)$  achieves the dual benefit of robustness and high performance—it eliminates the need for manual hyperparameter tuning while dynamically aligning the learning objective with the agent’s capabilities.

We also evaluate the impact of different threshold configurations in our adaptive weighting mechanism and hyperparameter configurations in DC component (see **Appendix C**).

## Conclusion

We presented ACDC, a hierarchical framework for on-line GCRL that integrates adaptive curriculum planning with dynamic contrastive control. By dynamically balancing the agent’s exploration and exploitation while regulating experience selection through contrastive representations, ACDC enables structured, stage-wise policy optimization. Extensive experiments across diverse robotic manipulation tasks demonstrate that our approach consistently outperforms state-of-the-art baselines, achieving superior sample efficiency and final success rates.

## Future Work

Our experiments primarily focus on robotic manipulation tasks with moderate-horizon planning (e.g., *HandManipulateEgg*, *HandManipulateBlock*). In preliminary experiments on long-horizon navigation tasks such as *AntMaze*, we observed less pronounced performance improvements. We attribute this limitation to the difficulty of effective initial exploration in extremely long-horizon settings, which remains a fundamental challenge in online GCRL. In future work, we plan to extend our framework to offline and offline-to-online GCRL settings, where diverse datasets with varying quality levels naturally align with ACDC’s curriculum design and may enable even stronger performance gains.

## References

Andrychowicz, M.; Wolski, F.; Ray, A.; Schneider, J.; Fong, R.; Welinder, P.; McGrew, B.; Tobin, J.; Abbeel, P.; and Zaremba, W. 2017. Hindsight Experience Replay. In *Advances in Neural Information Processing Systems*, volume 30, 5048–5058.

- Bengio, Y.; Louradour, J.; Collobert, R.; and Weston, J. 2009. Curriculum Learning. In *Proceedings of the 26th Annual International Conference on Machine Learning*, 41–48.
- Billard, A.; and Kragic, D. 2019. Trends and challenges in robot manipulation. *Science*, 364(6446): eaat8414.
- Borodin, A. 2009. Determinantal Point Processes. arXiv:0911.1153.
- Brockman, G.; Cheung, V.; Pettersson, L.; Schneider, J.; Schulman, J.; Tang, J.; and Zaremba, W. 2016. OpenAI Gym. arXiv:1606.01540.
- Chen, T.; Kornblith, S.; Norouzi, M.; and Hinton, G. 2020. A Simple Framework for Contrastive Learning of Visual Representations. In *Proceedings of the 37th International Conference on Machine Learning*, 1597–1607.
- Dai, T.; Liu, H.; Arulkumar, K.; Ren, G.; and Bharath, A. A. 2021. Diversity-Based Trajectory and Goal Selection with Hindsight Experience Replay. In *Proceedings of the Pacific Rim International Conference on Artificial Intelligence*, 32–45. Springer.
- Dey, R.; and Salem, F. M. 2017. Gate-variants of gated recurrent unit (GRU) neural networks. In *2017 IEEE 60th international midwest symposium on circuits and systems (MWSCAS)*, 1597–1600. IEEE.
- Eysenbach, B.; Zhang, T.; Salakhutdinov, R.; and Levine, S. 2022. Contrastive Learning as Goal-Conditioned Reinforcement Learning. In *Proceedings of the 36th International Conference on Neural Information Processing Systems*, 35330–35343.
- Fang, M.; Zhou, C.; Shi, B.; Gong, B.; Xu, J.; and Zhang, T. 2018. DHER: Hindsight Experience Replay for Dynamic Goals. In *Proceedings of the 6th International Conference on Learning Representations*.
- Fang, M.; Zhou, T.; Du, Y.; Han, L.; and Zhang, Z. 2019. Curriculum-guided Hindsight Experience Replay. In *Advances in Neural Information Processing Systems*, volume 32, 12623–12634.
- Florensa, C.; Held, D.; Wulfmeier, M.; Zhang, M.; and Abbeel, P. 2017. Reverse Curriculum Generation for Reinforcement Learning. In *Conference on Robot Learning*, 482–495.
- Haarnoja, T.; Zhou, A.; Abbeel, P.; and Levine, S. 2018. Soft Actor-Critic: Off-Policy Maximum Entropy Deep Reinforcement Learning with a Stochastic Actor. In *Proceedings of the 35th International Conference on Machine Learning*, 1861–1870. PMLR.
- Hadsell, R.; Chopra, S.; and LeCun, Y. 2006. Dimensionality Reduction by Learning an Invariant Mapping. In *Proceedings of the IEEE Conference on Computer Vision and Pattern Recognition*, 1735–1742.
- Han, Z.; Zhao, K.; Yu, Y.; Zhou, Y.; Li, J.; and Ma, Y. 2024. DATD3: Depthwise Attention Twin Delayed Deep Deterministic Policy Gradient For Model Free Reinforcement Learning Under Output Feedback Control. arXiv:2405.23857.
- Haynes, D.; Corns, S.; and Venayagamoorthy, G. K. 2012. An exponential moving average algorithm. In *2012 IEEE congress on evolutionary computation*, 1–8. IEEE.
- Karaman, S.; and Frazzoli, E. 2011. Sampling-based algorithms for optimal motion planning. *The international journal of robotics research*, 30(7): 846–894.
- Kim, T.; Kang, T.; Jeong, H.; and Har, D. 2024. Clustering-Based Failed Goal Aware Hindsight Experience Replay. *PeerJ Computer Science*, 10: e2588.
- Kulesza, A.; and Taskar, B. 2012. Determinantal Point Processes for Machine Learning. *Foundations and Trends in Machine Learning*, 5(2–3): 123–286.
- La Valle, S. M. 2011. Motion planning. *IEEE Robotics & Automation Magazine*, 18(2): 108–118.
- Laskin, M.; Srinivas, A.; and Abbeel, P. 2020. CURL: Contrastive Unsupervised Representations for Reinforcement Learning. In *Proceedings of the 37th International Conference on Machine Learning*, 5639–5650.
- LaValle, S. 1998. Rapidly-exploring random trees: A new tool for path planning. *Research Report 9811*.
- Lee, M. H.; and Moon, J. 2023. Deep Reinforcement Learning-Based Model-Free Path Planning and Collision Avoidance for UAVs: A Soft Actor-Critic with Hindsight Experience Replay Approach. *ICT Express*, 9(3): 403–408.
- Lillicrap, T. P.; Hunt, J. J.; Pritzel, A.; Heess, N.; Erez, T.; Tassa, Y.; Silver, D.; and Wierstra, D. 2015. Continuous Control with Deep Reinforcement Learning. arXiv:1509.02971.
- Lin, X.; Baweja, H.; Kantor, G.; and Held, D. 2019. Adaptive Auxiliary Task Weighting for Reinforcement Learning. In *Advances in Neural Information Processing Systems*, volume 32, 4772–4783.
- Liu, M.; Zhu, M.; and Zhang, W. 2022. Goal-Conditioned Reinforcement Learning: Problems and Solutions. In *Proceedings of the Thirty-First International Joint Conference on Artificial Intelligence*, 5502–5510. International Joint Conferences on Artificial Intelligence Organization.
- Martín-Martín, R.; Lee, M. A.; Gardner, R.; Savarese, S.; Bohg, J.; and Garg, A. 2019. Variable impedance control in end-effector space: An action space for reinforcement learning in contact-rich tasks. In *2019 IEEE/RSJ international conference on intelligent robots and systems (IROS)*, 1010–1017. IEEE.
- Matiisen, T.; Oliver, A.; Cohen, T.; and Schulman, J. 2019. Teacher-Student Curriculum Learning. In *Proceedings of the 36th International Conference on Machine Learning*, 4425–4434.
- Nair, A. V.; Pong, V.; Dalal, M.; Bahl, S.; Lin, S.; and Levine, S. 2018. Visual Reinforcement Learning with Imagined Goals. In *Advances in Neural Information Processing Systems*, volume 31, 9191–9200.
- Orthey, A.; Chamzas, C.; and Kavraki, L. E. 2023. Sampling-based motion planning: A comparative review. *Annual Review of Control, Robotics, and Autonomous Systems*, 7.
- Puterman, M. L. 1994. *Markov Decision Processes: Discrete Stochastic Dynamic Programming*. New York, NY, USA: John Wiley & Sons.

- Schaul, T.; Horgan, D.; Gregor, K.; and Silver, D. 2015. Universal Value Function Approximators. In *Proceedings of the 32nd International Conference on Machine Learning*, 1312–1320.
- Schaul, T.; Quan, J.; Antonoglou, I.; and Silver, D. 2016. Prioritized Experience Replay. In *International Conference on Learning Representations*.
- Sutton, R. S.; Barto, A. G.; et al. 1998. *Reinforcement learning: An introduction*, volume 1. MIT press Cambridge.
- Toussaint, M. 2015. Logic-Geometric Programming: An Optimization-Based Approach to Combined Task and Motion Planning. In *IJCAI*, 1930–1936.
- van den Oord, A.; Li, Y.; and Vinyals, O. 2018. Representation Learning with Contrastive Predictive Coding. arXiv:1807.03748.
- Wu, J.; Zhang, K.; Li, S.; Wang, Y.; and Yang, X. 2024. Prioritized Experience Replay Based on Dynamics Priority. *Scientific Reports*, 14: 5979.
- Yamashita, R.; Nishio, M.; Do, R. K. G.; and Togashi, K. 2018. Convolutional neural networks: an overview and application in radiology. *Insights into imaging*, 9(4): 611–629.
- Zhao, R.; and Tresp, V. 2018. Energy-Based Hindsight Experience Prioritization. In *Proceedings of the Conference on Robot Learning*, 113–122.
- Zheng, C.; Eysenbach, B.; Walke, H.; Yin, P.; Fang, K.; and Salakhutdinov, R. 2023. Stabilizing Contrastive RL: Techniques for Robotic Goal Reaching from Offline Data. arXiv:2306.03346.

## Appendix A: Hyperparameter in AC Module

In this section, we empirically justify the hyperparameter choices in the Adaptive Curriculum (AC) module, including the sliding window size used for diversity estimation, the sensitivity parameter  $\sigma$  in the quality scoring function, and the growth factors governing the weighting scheme.

### A.1 Sliding Window Size (Eq. 4)

The sliding window size determines the temporal resolution for diversity calculation using DPPs (Kulesza and Taskar 2012). We evaluated window sizes  $w \in \{2, 3, 4, 5\}$  on the *HandManipulateBlockFull* task.

Table 3: Grid search for sliding window size. Smaller windows ( $w = 2$ ) capture fine-grained local dynamics essential for manipulation, whereas larger windows dilute local correlations.

| Window Size ( $w$ ) | Mean Success Rate                 | Convergence Epoch |
|---------------------|-----------------------------------|-------------------|
| <b>2 (Default)</b>  | <b><math>0.25 \pm 0.04</math></b> | <b>85</b>         |
| 3                   | $0.21 \pm 0.03$                   | 92                |
| 4                   | $0.18 \pm 0.04$                   | >100              |
| 5                   | $0.19 \pm 0.02$                   | >100              |

### A.2 Sensitivity Parameter $\sigma$ (Eq. 7)

The parameter  $\sigma$  in Eq(7) controls the "strictness" of the goal achievement evaluation, effectively shaping the gradient of the quality metric. We evaluated  $\sigma \in \{0.05, 0.1, 0.2, 0.5\}$  in different environments to find the optimal balance between discrimination and signal density.

Table 4: Sensitivity analysis of  $\sigma$  on *HandManipulateEggFull*. The default value  $\sigma = 0.2$  achieves the highest success rate by effectively balancing gradient strength and discriminative power.

| Sensitivity ( $\sigma$ ) | Mean Success Rate                 | Convergence Behavior         |
|--------------------------|-----------------------------------|------------------------------|
| 0.05                     | $0.42 \pm 0.03$                   | Stalled (Gradient Vanishing) |
| 0.1                      | $0.48 \pm 0.05$                   | Slow / Unstable              |
| <b>0.2 (Default)</b>     | <b><math>0.69 \pm 0.05</math></b> | <b>Stable Convergence</b>    |
| 0.5                      | $0.61 \pm 0.06$                   | Early Plateau (Noisy)        |

- $\sigma \in \{0.05, 0.1\}$ : **Too strict (Under-estimation)**. The Gaussian kernel decays too rapidly, causing even near-optimal trajectories to receive negligible scores. This results in vanishing gradients for the quality metric, stalling the curriculum progress.
- $\sigma = 0.2$  (**Selected**): **Optimal Balance**. This value provides the most effective shaping, distinguishing "close calls" from total failures while maintaining non-zero gradients for trajectories approaching the goal.
- $\sigma = 0.5$ : **Too lenient (Over-estimation)**. The kernel is too wide, assigning misleadingly high scores to failed trajectories far from the goal. This reduces the discriminative power of the quality metric and introduces noise into the curriculum planning.

As shown in Table 4, quantitative results on the *HandManipulateEggFull* task confirm this analysis, demonstrating that  $\sigma = 0.2$  yields superior performance compared to other settings.

### A.3 Adaptive Growth Factors (Eq. 11)

We formulated the growth rate  $\eta(s_r)$  with multipliers (0.5, 1.0, 2.0) corresponding to the Struggling, Learning, and Mastery phases. We compared this against a linear growth strategy (constant 1.0) and a more aggressive step strategy (0.2, 1.0, 5.0).

Table 5: Comparison of growth factor strategies. The proposed moderate exponential growth ensures stable transitions between exploration and exploitation.

| Strategy                        | Final Success (BlockFull)         |
|---------------------------------|-----------------------------------|
| Linear (1.0, 1.0, 1.0)          | $0.15 \pm 0.03$                   |
| Aggressive (0.2, 1.0, 5.0)      | $0.23 \pm 0.05$                   |
| <b>Proposed (0.5, 1.0, 2.0)</b> | <b><math>0.25 \pm 0.04</math></b> |

## Appendix B: Experiment Analysis

### B.1 Extended Convergence on BlockFull

Standard benchmarks typically run for 100 epochs. However, for complex contact-rich task *HandManipulateBlockFull*, this duration may be insufficient to observe the full asymptotic behavior of the algorithms. To verify the long-term convergence properties, we extended the training horizon to 250 epochs.

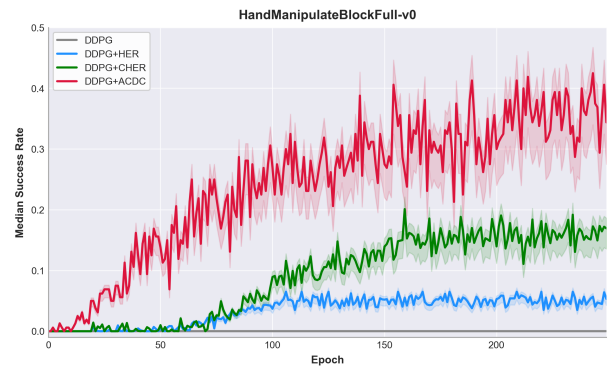


Figure 10: Extended convergence analysis (250 epochs) on *HandManipulateBlockFull*.

As illustrated in Figure 10, the performance gap widens significantly beyond the standard 100-epoch mark. Standard baselines exhibit severe exploration stagnation: DDPG (Lillicrap et al. 2015) fails completely (0.0 success), while DDPG+HER (Andrychowicz et al. 2017) and DDPG+CHER (Fang et al. 2019) plateau at negligible success rates ( $\approx 5\%$  and  $\approx 15\%$ , respectively), indicating an inability to escape local optima. In contrast, ACDC successfully breaks this exploration bottleneck.

## B.2 Sample Efficiency and Regret Analysis

To provide a comprehensive evaluation of sample efficiency beyond final asymptotic performance, we introduce two quantitative metrics: *Time-to-Threshold (TTT)* and *Cumulative Regret (R)*.

*Time-to-Threshold (TTT)* is defined as the number of epochs required for an agent to first reach a pre-defined success rate threshold  $\theta$ . This metric directly reflects the convergence speed.

*Cumulative Regret (R)* quantifies the total learning cost throughout the training horizon  $T$  (Sutton, Barto et al. 1998), formalized as:

$$R = \sum_{t=1}^T (1 - s_{r_t}), \quad (19)$$

where  $s_{r_t}$  denotes the success rate at epoch  $t$ . A lower regret value indicates that the agent converges with fewer failure interactions during the exploration process.

Table 2 demonstrates that ACDC achieves superior sample efficiency across diverse task complexities. Regarding *Time-to-Threshold (TTT)*, ACDC significantly accelerates convergence speed. In PickAndPlace, it reduces TTT to **18 epochs**, representing a  $\sim 48\%$  **speedup** over the standard HER baseline (35 epochs) and a **55% speedup** over DTGSH (40 epochs). This advantage widens in high-dimensional tasks like HandReach, where ACDC reaches the threshold in just **5 epochs**— $7\times$  **faster** than the strongest baseline (DTGSH, 35 epochs). Crucially, for the bottleneck task BlockFull, ACDC is the sole method to successfully reach the threshold (**TTT=75**), whereas all baselines fail to converge.

In terms of *Cumulative Regret (R)*, ACDC consistently incurs the lowest learning cost throughout the training horizon. It reduces regret by over **55%** in PickAndPlace (**18.2** vs. 41.2 for DTGSH). Even in *HandManipulateBlockFull*, where baselines suffer near-maximum regret ( $> 95$ ), ACDC effectively lowers the cost to **88.5**.

## B.3 SAC Agent Experiments

To demonstrate the robustness of the ACDC framework across different policy types, we integrated it with Soft Actor-Critic (SAC) (Haarnoja et al. 2018), a stochastic maximum entropy off-policy algorithm. We evaluated performance on four challenging Hand manipulation environments.

Table 6: Mean success rate  $\pm$  standard deviation averaged over the last 5 epochs across Hand manipulation tasks. Best results are shown in **bold**.

| Method          | BlockFull                         | EggFull                           | PenRotate                         | HandReach                         |
|-----------------|-----------------------------------|-----------------------------------|-----------------------------------|-----------------------------------|
| SAC (Base)      | 0.00 $\pm$ 0.00                   | 0.00 $\pm$ 0.00                   | 0.02 $\pm$ 0.02                   | 0.00 $\pm$ 0.00                   |
| SAC+HER         | 0.02 $\pm$ 0.02                   | 0.09 $\pm$ 0.03                   | 0.19 $\pm$ 0.03                   | 0.56 $\pm$ 0.09                   |
| <b>SAC+ACDC</b> | 0.09 $\pm$ 0.02                   | 0.37 $\pm$ 0.04                   | <b>0.31 <math>\pm</math> 0.03</b> | 0.68 $\pm$ 0.09                   |
| DDPG+ACDC       | <b>0.12 <math>\pm</math> 0.02</b> | <b>0.53 <math>\pm</math> 0.04</b> | 0.23 $\pm$ 0.02                   | <b>0.76 <math>\pm</math> 0.04</b> |

As shown in Figure 11 and Table 6, the vanilla SAC agent fails completely due to the sparse reward signal. While integrating HER (SAC+HER) enables basic learning, it struggles with complex manipulation tasks, achieving only  $0.02 \pm 0.02$  success rate in BlockFull and  $0.09 \pm 0.03$  in EggFull. In

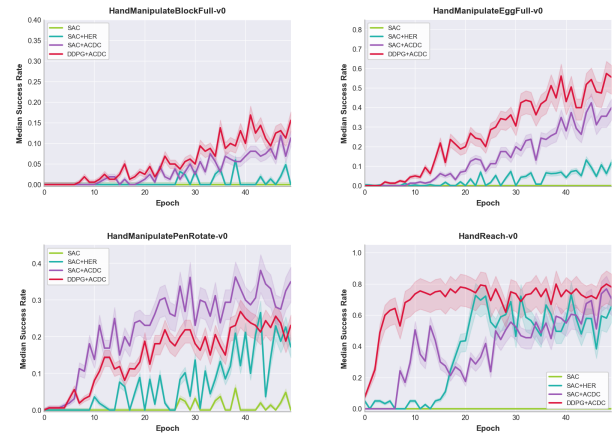


Figure 11: Learning curves comparing SAC, SAC+HER, SAC+ACDC, and DDPG+ACDC on Hand environments.

contrast, SAC+ACDC significantly outperforms SAC+HER across all tasks. Notably, in EggFull, ACDC quadruples the success rate (0.37 vs. 0.09), and in BlockFull, it successfully initiates learning (0.09) where SAC+HER stagnates. This confirms that ACDC’s curriculum planning and contrastive selection provide critical guidance for stochastic policies in high-dimensional exploration.

Comparing the two ACDC variants reveals that the framework functions effectively regardless of the underlying RL algorithm, though their relative performance varies depending on the specific task characteristics. In PenRotate, SAC+ACDC ( $0.31 \pm 0.03$ ) outperforms DDPG+ACDC ( $0.23 \pm 0.02$ ). This superiority suggests that SAC’s maximum entropy objective encourages more expansive stochastic exploration in rotational goal spaces, which synergizes with ACDC’s diversity metric to facilitate the discovery of viable rotation trajectories.

In contrast, DDPG+ACDC maintains a significant edge in EggFull ( $0.53 \pm 0.04$  vs.  $0.37 \pm 0.04$ ). This is attributed to the lower variance of deterministic policy gradients, which provide the precision and stability required for complex, contact-rich manipulation once a high-quality path is identified. In high-difficulty benchmarks like BlockFull and HandReach, both variants achieve comparable results as shown in Table 6, suggesting that the benefits of ACDC are robust across different actor-critic architectures. These results validate ACDC as a generalized framework where performance variations reflect the natural synergy between a base algorithm’s exploration strategy and the specific geometric constraints of the task.

## Appendix C: Ablation Studies

### C.1 Threshold Sensitivity and Robustness

We evaluate the impact of different threshold configurations ( $\theta_{low}, \theta_{high}$ ) in the adaptive curriculum mechanism. As illustrated by the sensitivity analysis in Figure 12, the framework exhibits remarkable robustness to variations in these parameters, with performance remaining stable across a wide effective range.

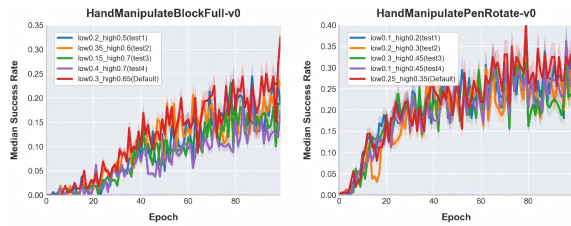


Figure 12: Threshold sensitivity analysis across different  $\theta_{low}$  and  $\theta_{high}$  configurations.

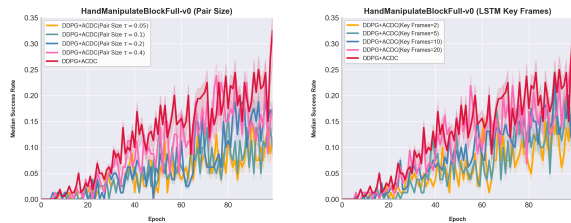


Figure 13: Ablation study on hyperparameter sensitivity. Left: Impact of contrastive pair threshold  $\tau$ . Right: Effect of LSTM key frames  $\mathcal{K}$ .

This suggests that the thresholds are designed to loosely categorize the curriculum learning process into three logical phases — Exploration, Balance, and Exploitation — rather than to serve as strict, sensitive boundaries. The high degree of robustness indicates that the specific threshold values are less critical than the existence of the curriculum structure itself, which facilitates a smooth transition in experience prioritization as the agent progresses. Consequently, the chosen default values are simply empirical representatives that align with the agent’s natural learning trajectory. This structural stability ensures that ACDC can be deployed across diverse environments without the need for exhaustive hyperparameter tuning.

## C.2 Hyperparameter Configuration

We perform experiments to validate our hyperparameter choices for the DC component, specifically examining contrastive pair threshold  $\tau$  and LSTM key frames  $\mathcal{K}$  in the BlockFull environment.

As shown in Figure 13 (left), we evaluate  $\tau \in \{0.05, 0.1, 0.2, 0.4\}$  against our default configuration ( $\tau = 0.3$ ). Smaller thresholds ( $\tau \in \{0.05, 0.1, 0.2\}$ ) consistently underperform, achieving mean success rates of  $0.088 \pm 0.023$ ,  $0.101 \pm 0.032$ , and  $0.165 \pm 0.024$  over the last 20 epochs respectively, compared to  $0.247 \pm 0.052$  for the default setting.  $\tau = 0.4$  achieves comparable performance, but requires additional epochs to reach similar performance levels.

Figure 13 (right) examines the impact of key frame selection for LSTM encoding. We compare random sampling strategies with  $|\mathcal{K}| \in \{2, 5, 10, 20\}$  frames (all including start and end achieved goals, with remaining frames randomly selected) against our default strategic sampling. Using too few frames ( $|\mathcal{K}| \in \{2, 5\}$ ) limits temporal context,

achieving only  $0.125 \pm 0.037$  and  $0.138 \pm 0.045$  respectively. Larger frame counts ( $|\mathcal{K}| \in \{10, 20\}$ ) exhibit higher variance ( $0.169 \pm 0.036$  and  $0.188 \pm 0.052$ ) and less stable learning abilities. Our strategic configuration optimally balances temporal coverage with training stability, achieving superior performance of  $0.247 \pm 0.052$ .